Natural Resources Research, Vol. 29, No. 1, February 2020 (© 2019)
https://doi.org/10.1007/s11053-019-09560-y

Original Paper

Exploring Spatially Non-stationary Relationships in the Determinants of Mineralization in 3D Geological Space

Jixian Huang,[1] Xiancheng Mao,[1] Jin Chen,[1,2] Hao Deng,[1] Jeffrey M. Dick,[1] and Zhankun Liu[1]

Received 25 June 2019; accepted 14 September 2019
Published online: 23 September 2019

Exploring the spatial relationships between various geological features and mineralization is not only conducive to understanding the genesis of ore deposits but can also help to guide mineral exploration by providing predictive mineral maps. However, most current methods assume spatially constant determinants of mineralization and therefore have limited applicability to detecting possible spatially non-stationary relationships between the geological features and the mineralization. In this paper, the spatial variation between the distribution of mineralization and its determining factors is described for a case study in the Dingjiashan Pb–Zn deposit, China. A local regression modeling technique, geological weighted regression (GWR), was leveraged to study the spatial non-stationarity in the 3D geological space. First, ordinary least-squares (OLS) regression was applied, the redundancy and significance of the controlling factors were tested, and the spatial dependency in Zn and Pb ore grade measurements was confirmed. Second, GWR models with different kernel functions in 3D space were applied, and their results were compared to the OLS model. The results show a superior performance of GWR compared with OLS and a significant spatial non-stationarity in the determinants of ore grade. Third, a non-stationarity test was performed. The stationarity index and the Monte Carlo stationarity test demonstrate the non-stationarity of all the variables throughout the area. Finally, the influences of the degree of non-stationary of all controlling factors on mineralization are discussed. The existence of significant non-stationarity of mineral ore determinants in 3D space opens up an exciting avenue for research into the prediction of underground ore bodies.

KEY WORDS: Geographically weighted regression, Spatial non-stationarity, Metallogenic prognosis, 3D geological space, Ordinary least-squares (OLS) regression.

INTRODUCTION

With the current interest in deep mine prospecting and the ongoing improvements to subsurface geological and geophysical mapping methods (Schamper et al. 2014a, b; Chen and Wu 2017), vast amounts of geological exploration data in three dimensions are being generated. Analysis and modeling of 3D geological objects by integrating

[1]Key Laboratory of Metallogenic Prediction of Nonferrous Metals and Geological Environment Monitoring (Ministry of Education), School of Geosciences and Info-Physics, Central South University, Changsha 410083, China.
[2]To whom correspondence should be addressed; e-mail: chenjin215@hotmail.com

geophysical and geological datasets provides new insights into exploration targeting, but uncertainty in mineral exploration cannot be eliminated (Lindsay et al. 2012; Zuo and Xiong 2018; Wang et al. 2015; Li et al. 2019). How to use these large three-dimensional datasets to reveal the spatial distribution of the mineralization and the determinants of ore genesis is becoming an important research topic in metallogeny.

The goal of this research is to uncover something new about ''why things are the way they are.'' Exploring the spatial relationships between various geological features and mineralization is not only useful in understanding the ore genesis of deposits but can also help to guide mineral exploration by providing predictive mineral maps (Liu et al. 2013). Recently, spatial issues associated with mineralization and its determining factors have been of interest to many geologists. Most current methods are based on models that assume that the determinants of mineralization are constant over space (Zhang et al. 2012; Chen et al. 2005; Mao et al. 2009, 2010; Lin et al. 2019; Chen et al. 2019). Such models can only produce ''average'' or ''global'' parameter estimates (Batisani and Yarnal 2009; Geri and Amici 2010) and are unable to detect possible spatial non-stationary relationships. If spatial non-stationarity in the processes affecting ore mineralization exists, predictive modeling based on these classical global statistical methods will have limited accuracy.

In past research that aimed to explore spatial trends and non-stationary, a series of statistical techniques and modeling approaches were proposed. The solutions have focused on local spatial analysis and spatial modeling (Zhang et al. 2018). Early contributions introduced location coordinates or their functions as direct or indirect independent variables in predictive models to express linear or nonlinear trends in space (Agterberg, 1964, 1970; Casetti, 1972). The famous local window statistics models in geosciences, such as local singularity analysis, reduce the effect of spatial non-stationarity to some degree by removing spatial trends and minimizing the effects of high and low values of the variables on predictions (Cheng 1997, 1999; Zuo et al. 2016; Zhang et al. 2016). Geographically weighted regression (GWR) is a recently developed spatial analysis technique that considers the non-stationarity of variables. It is a relatively simple, but effective technique for exploring spatially varying relationships (Fotheringham et al. 1996, 1998, 1999; Brunsdon et al. 1996, 1999). It has attracted a great deal of attention in different fields such as resources and environment (Tu and Xia 2008; Gao and Li 2011; Gilbert and Chakraborty 2011; Clement et al. 2009; Harris and Brunsdon 2010; Zhao et al. 2014; Zhang et al. 2019), and economics (Lu et al. 2011; Lu and Bo 2014; Lee and Schuett 2014; Nilsson 2014; Breetzke and Cohn 2012; Andrew et al. 2015). In the field of metallogenic prediction, Zhang et al. (2018) developed a spatially weighted logistic regression technique where the dependent variable is a binary variable. Liu et al. (2013) quantified the spatial relationships between gold mineralization and plausible controlling factors in the central part of the St Ives area, Western Australia. Zhao et al. (2014) applied geographically weighted regression to identify spatially non-stationary relationships between Fe mineralization and its controlling factors in eastern Tianshan, China.

While GWR shows strength in modeling non-stationary spatial relationships, most of the existing work is limited to two-dimensional (2D) space. Tobler's first law of geography (Tobler 1979), which argues that ''everything is related to everything else, but near things are more related than distant things,'' applies equally to 3D geological space. Therefore, the influence of ore-controlling factors on mineralization is multidimensional. In the metallogenic system, there are great differences in the distribution of geological bodies and fluids at different depths, temperature, pressure, acidity and alkalinity, and redox environment. The spatial non-stationarity of mineralization in the vertical direction cannot be ignored. Therefore, modelers need to introduce variables that reflect spatial non-stationarity at different depths.

Given that real geological space is a three-dimensional (3D) space, extension of the GWR to 3D will give us a new perspective to explore spatially non-stationary relationships in the determinants of mineralization. In this study, we extend the current GWR model from 2D to 3D. The main advantage of the 3D GWR is that it can simulate the spatial relationships between the mineralization and its determinants in real geological space. The spatial relationships can be quantified and calculated by using the 3D GWR model, and the geological information obtained from the simulation results has three-dimensional attributes. To examine the use of GWR in 3D space to detect spatially non-stationary relationships between mineral concentration and its determinants, we performed a case study of the Dingjiashan Pb–Zn deposit by using the ore grades of Zn and Pb as the dependent variables and

potential determinants as explanatory variables in the regression. After investigating the adaptability of GWR in modeling the relationships between the mineralization and its driving factors, we applied the GWR to the 3D ore deposit and made some comparisons with the predictions. Finally, we discussed the degree of non-stationary influence for all the controlling factors on mineralization.

The main original contributions of this study can be summarized as follows:

- We introduced a new method to analyze quantitatively the spatial relationship among the complex geological factors in real 3D space. This innovation will contribute to the techniques of metallogenic prediction.
- We extended the GWR model from 2D to 3D space and implemented it in the MATLAB language.
- We applied the GWR model in 3D geological space to explore the spatial relationships between mineralization and its controlling factors.

DATA

Study Area

The approach proposed in this paper was tested on the Dingjiashan Pb–Zn deposit, which is a nonferrous mine and is well known for its polymetallic mineralization. It is located in the northeastern part of the Wuyi–Yunkai fold belt in the eastern region of the South China fold system. The study area measures 880 m from east to west, 730 m from south to north, and has depth of 375 m based on elevation change from − 75 m to 285 m above sea level. The Pb–Zn ore in this district occurs in one of the largest deposits in eastern China (Fig. 1) (Zhang et al. 2011). The exposed strata are mainly Mesozoic, continental magmatic rocks, which are underlain by middle and upper Proterozoic metamorphic rocks. The geological structure of the district includes many folds, faults, and unconformities.

Data and Variables

In this study, we choose mineralization, which is measured by the ore grades of Zn and Pb as the dependent variables. Figure 2 shows the three-dimensional spatial distribution of the grades of Zn (a) and Pb (b) ore. The explanatory variables are selected based on a block model of the region, which was built using the Datamine (Changsha, Hunan province, China) software in a geocentric 3D coordinate system. The block model consists of a set of regular blocks or units, or voxels. Each voxel has attributes, such as grade and stratigraphic types. The geological space is divided into three-dimensional voxels whose size is 10 m × 10 m × 10 m. Each voxel has values for ore concentration and each potential explanatory variable (Shao et al. 2010). In this study, the coordinates of each voxel correspond to its center point.

For each voxel that includes data for samples, the Zn or Pb grade is calculated as the weighted average grade, measured as the length-weighted mean of samples in the voxel. It is calculated as follows:

$$C = \sum_{i=1}^{n} C_i H_i / \sum_{i=1}^{n} H_i \quad (x_i, y_i, z_i) \in v$$

where C_i is Zn or Pb content of sample i, H_i is the length of sample i, (x_i, y_i, z_i) represents the coordinates of the center point, and v represents the voxel space. The ore grade of voxels that do not include samples is obtained by kriging interpolation.

In this study, the explanatory variables were selected to represent the determinants of mineralization. The variables are a series of quantified ore-controlling factors based on various geological conditions and were originally chosen for Pb–Zn deposit metallogenic prognosis in which high accuracy was obtained by comparison with the measured data (Shao et al. 2010; Zhang et al. 2011; Mao et al. 2016). A detailed description of all the variables is given in Table 1.

A comprehensive analysis of the distribution of macroscale mineralization and emplacement of ore deposits and orebodies together with information on metallogenic evolution, ore genesis, and source of ore-forming materials shows that the Dingjiashan Pb–Zn deposit is jointly controlled by magmatic activities associated with the emplacement of granitoid rocks, stratigraphic fabrics and lithology, tectonic deformation, and important geological interfaces in the early and late Yanshanian period (Shao et al. 2010). The ore-controlling factors are selected mainly according to the stratigraphy expressed as the quantified factor dZ1L3_Z1L2,

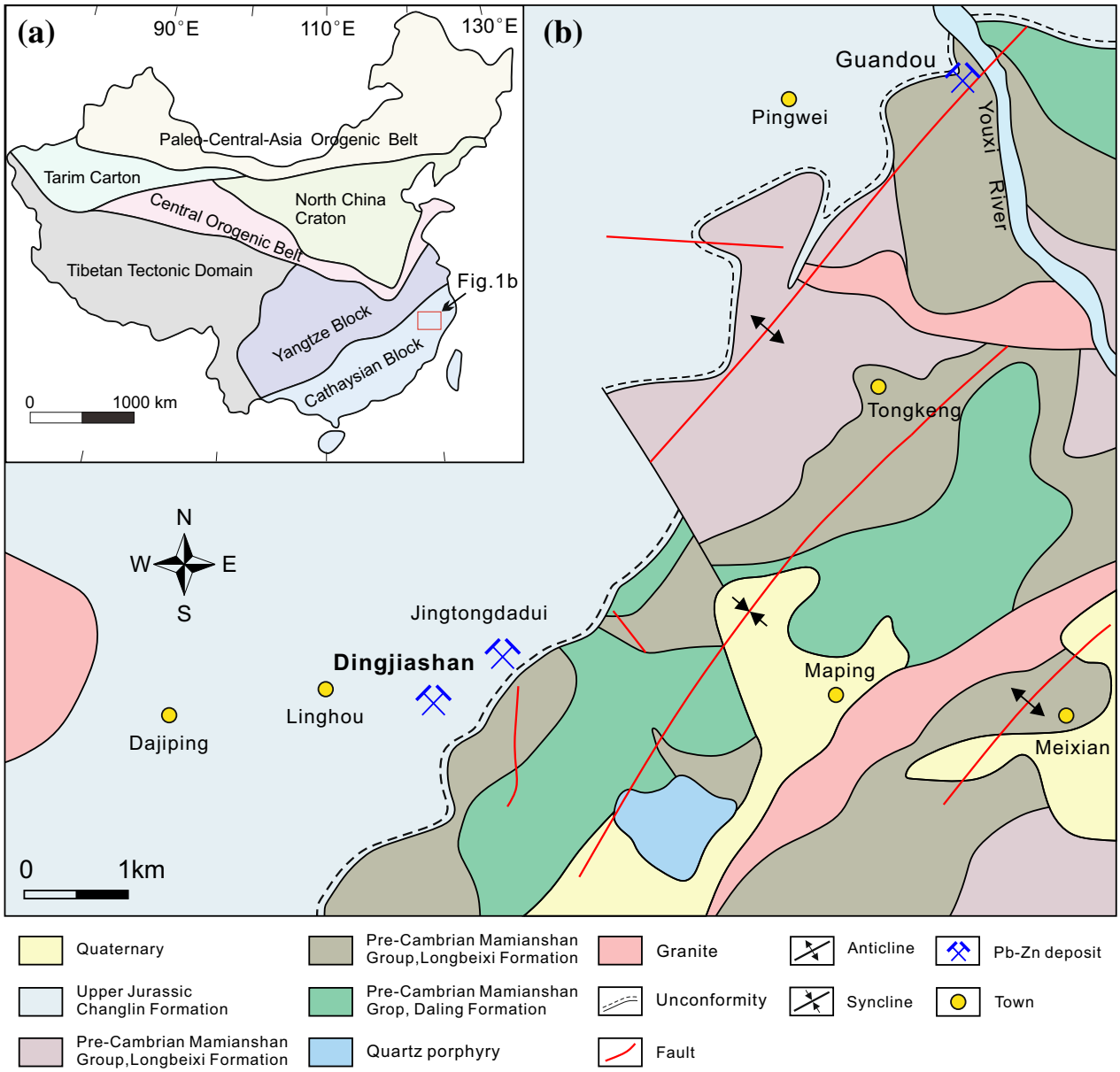

Figure 1. Geological map of the Dingjiashan Pb–Zn deposit (Zhang et al. 2011).

unconformity surface structure described by the quantified factors dU, gU, aU_S, waU, and wbU, and folds and buried uplifts of ore-bearing rock series under volcanic caprock, which are represented by the quantified factors waZ1L3_Z1L2 and wbZ1L3_Z1L2. These quantified ore-controlling factors are described as follows (Mao et al. 2016; Shao et al. 2010):

dU, the distance field of the unconformity surface, is measured as the minimum distance from the voxel to the unconformity surface.

waU and wbU, the trend–undulation factors of the unconformity surface, which represent the effect of the undulation on its surrounding geological space, are measured by the Euclidean distance from the voxel to the trend of the nearest unconformity

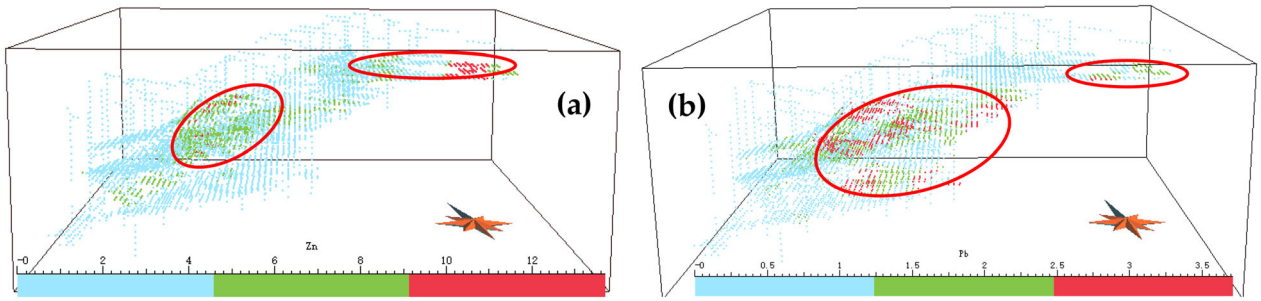

Figure 2. Spatial distribution of ore grade: (**a**) Zn and (**b**) Pb.

Table 1. Description of variables

Variable	Definition	Number of data points	Minimum	Maximum	Mean	Standard deviation
Zn	Grade of zinc ore	5944	.0000	13.7083	3.0364	2.5003
Pb	Grade of lead ore	5944	0.0000	11.7583	0.9352	1.0785
dU	Distance to the unconformity surface	5944	− 153.3820	158.1579	− 31.8236	41.1199
dz1L3_Z1L2	Distance to the stratigraphical boundary	5944	− 68.9773	184.4332	31.9992	39.7008
aU_S	Angle of the unconformity surface	5944	14.1148	75.8935	33.5551	19.3764
gU	Slope of the unconformity surface	5944	.9041	73.4875	26.4079	14.2816
waU	First-degree trend–undulation factor of the unconformity surface	5944	− 36.6321	27.9674	− 1.5189	7.2718
wbU	Second-degree trend–undulation factor of the unconformity surface	5944	− 28.4701	12.8811	-.3519	6.3120
waZ1L3_Z1L2	First-degree trend of the stratigraphical boundary	5944	− 20.5956	20.4773	.8451	5.880
wbZ1L3_Z1L2	Second-degree trend of the stratigraphical boundary	5944	− 14.1421	18.3306	-.4116	4.6067
X	*X* coordinate	5944	39,620,936	39,621,816	39,621,267	177.525
Y	*Y* coordinate	5944	2,903,415	2,904,145	2,903,779	142.569
Z	*Z* coordinate	5944	− 75	285	102.37	61.200

surface. Variable waU is the first-level undulation factor while wbU represents the second-level undulation factor (Mao et al. 2016; Shao et al. 2010).

gU is the slope of the unconformity. A steeply dipping unconformity is the most favorable structure for the late-stage reformation of strata-bound Pb–Zn deposits. As ore bodies on both sides of the steep unconformable structure show a trend of thickening and enrichment, the slope of the unconformity is very important to the mineralization. The variable gU is measured by the slope from the voxel to the nearest place on the unconformity surface.

aU_S is the angle of the unconformity. A large angle of intersection of the unconformity surface with the underlying greenschist strata is a favorable condition for mineralization. The angle of the unconformity is an important factor in metallogenesis, and the unconformity can intersect with multiple strata. The variable aU_S is measured with the closest angle between the voxel and the nearest distance to the unconformity surface.

dZ1L3_Z1L2 is the distance to the stratigraphic interface. The transition zone between the greenschist belt (Z1L3) and the light schist belt (Z1L2) is the most favorable ore-containing position of the strata-bound ore. This kind of ore-controlling factor of the stratum can be described by the distance to the Z1L3_Z1L2 stratigraphic interface. The variable dZ1L3_Z1L2 is measured as the minimum distance from the voxel to the Z1L3_Z1L2 stratigraphic

interface. The voxel value located above the Z1L3_Z1L2 stratigraphic interface is positive and below is negative.

waZ1L3_Z1L2 and wbZ1L3_Z1L2 are the trend–undulation factors of the stratigraphic interface (Mao et al. 2016; Shao et al. 2010). Folds and concealed uplift of ore rock under the volcanic rock can be expressed by the bending and fluctuating form of the interlayer interface of the ore rock. The variables waZ1L3_Z1L2 and wbZ1L3_Z1L2 represent the first-level and second-level degree of undulation of Z1L3_Z1L2 stratigraphic interface and are measured as the Euclidean distance from the voxel to the trend of the nearest place of the Z1L3_Z1L2 stratigraphic boundary.

Data Analysis Procedure

Five stages of analysis are undertaken in this study. In the first stage, an ordinary least-squared (OLS) regression model associating ore grade with eight explanatory variables is calibrated to generate a baseline global set of results and to examine potential multi-collinearity effects among any of the predictor variables. In the second stage, the GWR model is calibrated by using different kernel functions to explore possible spatial variation in the processes affecting ore concentration. In the third stage, the OLS and GWR results are analyzed and compared and an examination of spatial dependency in 3D space of the regression residuals from both models is presented. In the fourth stage, a spatial stationarity test is performed and the non-stationarity of different variables is demonstrated. Finally, the influences of the degree of non-stationarity of controlling factors on mineralization are discussed.

METHODS

Geographically Weighted Regression in 3D Space

In this paper, OLS regression and GWR were used to investigate the relationships between ore concentration and its determinants. GWR is an extension of the OLS model that allows local parameters to be estimated (Fotheringham et al. 2001, 2002; Brunsdon et al. 2002; Yao and Fotheringham 2015). The standard GWR formulation can be represented as:

$$y_i = \beta_0(u_i, v_i) + \sum_{j=1}^{k} \beta_j(u_i, v_i)x_{ij} + \varepsilon(u_i, v_i) \quad i = 1 \ldots n \tag{1}$$

where (u_i, v_i) is the 2D coordinate location of ith point, y_i is the estimated value of the dependent variable at point i, x_{ij} is the value of the variable x_j at point i, $\beta_0(u_i, v_i,)$ is the constant estimated for point i, $\beta_j(u_i, v_i,)$ represents the local parameter estimate for independent variable x_j at point i, and $\varepsilon(u_i, v_i)$ is the ith value of a normally distributed error vector with mean equal to zero.

In this paper, this model is extended to three-dimensional space as follows:

$$y_i = \beta_0(u_i, v_i, w_i) + \sum_{j=1}^{k} \beta_j(u_i, v_i, w_i)x_{ij} + \varepsilon(u_i, v_i, w_i) \quad i = 1 \ldots n \tag{2}$$

where (u_i, v_i, w_i) denotes the 3D coordinate location of ith point.

Parameter estimates in GWR are obtained by weighting all observations around a specific point i using a distance decay function, which based on their spatial proximity to it. The observations closer to point i have a greater influence on the local parameter estimates for the location and are weighted more than data located farther from point i. The parameters are estimated from:

$$\hat{\beta}(\mu, v, w) = \left(\boldsymbol{X}^T \boldsymbol{W}(\mu, v, w)\boldsymbol{X}\right)^{-1} \boldsymbol{X}^T \boldsymbol{W}(\mu, v, w)\boldsymbol{y} \tag{3}$$

where the bold type denotes a matrix, $\hat{\beta}(\mu, v, w)$ represents the unbiased estimate of $\boldsymbol{\beta}$, and $\boldsymbol{W}(\mu, v, w)$ is the weighting matrix, which acts to ensure that observations closer to the specific point have a higher weight. It can be determined by a kernel function.

There are two types of kernels. The fixed kernel assumes that the bandwidth at each regression point is a constant across the study area while the adaptive kernel permits use of a variable bandwidth and can adapt the bandwidth size to variations according to data density. As the data used in this study are unevenly distributed, the following two adaptive kernels are employed:

$$\text{bi-square: } w_{ij} = \left[1 - \left(d_{ij}/b\right)^2\right]^2 \text{ if } d_{ij} < b \\ = 0 \text{ otherwise} \quad (4)$$

$$\text{tri-cube: } w_{ij} = \left[1 - \left(d_{ij}^2/b^2\right)^3\right]^{3/2} \text{ if } d_{ij} < b \\ = 0 \text{ otherwise} \quad (5)$$

where w_{ij} represents the weight of observation j for point i, d_{ij} expresses the Euclidean distance between points i and j, N is the optimal number of nearest neighbors, and b is the distance to the Nth nearest neighbor, which governs the decay rate of w_{ij} and the degree of locality of the regression model. An appropriate number of nearest neighbors can be determined by minimizing the cross-validation (CV) or Akaike information criterion (AIC) scores (Fotheringham et al. 2002).

Non-stationarity Tests

Stationary Index

In this paper, we calculate the stationary index (Brunsdon et al. 1998) which is designed to measure the spatial non-stationarity of each variable. Values smaller than one indicate stationarity (Brunsdon et al. 2002).

The calculation includes three steps: First, the interquartile range of GWR local parameter estimates for each explanatory variable is computed; second, twice the standard error of the global estimates is obtained; finally, the ratio of these two factors is calculated as the stationary index. If the interquartile range is bigger than twice the standard error of the global mean, it may suggest that the relationship is non-stationary (Brunsdon et al. 2002).

Monte Carlo Stationarity Test

The Monte Carlo significance testing procedure employs a pseudo-random number generator to reallocate the observations across the spatial voxels. The Monte Carlo stationarity test is an approach to examine the validity of any inferences drawn from the local results (Fotheringham et al. 2002). The test result depends on the rank of the observed data relative to the random samples.

Given the number of local model calibrations n, the specific process in this paper is as follows (Yao and Fotheringham 2015):

(1) For each variable, obtain the local parameter estimates and compute the variance of the estimates.
(2) Rearrange data randomly and at the same time keep $y_i x_{1i} x_{2i} \ldots x_{ni}$ together.
(3) Perform the GWR calculation and compute a new set of local parameter estimates based on rearranged data.
(4) For each variable, calculate the variance of the local parameter estimates.
(5) Repeat steps (2) to (4) n times.
(6) For each variable, compare the variance of local parameter estimates in step (1) with those from steps (2) to (4), and calculate the p value associated with (1) which is the proportion of variances that lie above that for (1) in a list of variances sorted high to low.

RESULTS

Statistical Hypothesis tests and OLS Diagnosis

Data should be examined before further analysis. The results of statistical hypothesis testing are shown in Tables 2 and 3. All values of the variance inflation factor (VIF) in Table 2 are less than 7.5, which demonstrate that multi-collinearity among the explanatory variables does not exist. The indices for explanatory variables in Table 2, including the OLS model intercepts, indicate that the regression coefficients are statistically significant at the 95% confidence level, suggesting that all the explanatory variables are important in the regression model. The OLS model diagnostic results are demonstrated in Table 3. The joint F-statistic and joint Wald statistic listed in Table 3 indicate that the regression model is significant. The value of the Jarque–Bera statistic in Table 3 shows the abnormal distribution of residuals. The multiple R-squared of the model for Zn grade is 0.150 and that for Pb grade is 0.165. These values indicate that both models can only explain about 15% or 16.5% of the variation and cannot express the relationship between the distribution of

Table 2. Results of significance testing of coefficient variation

	Variable	Coefficient	StdError	*t*-Statistic	Probability	Robust_SE	Robust_t	Robust_Probability	VIF
Zn	Intercept	4.725241	0.132515	35.658254	0.000000*	0.162726	29.038039	0.000000*	–
	dU	0.015493	0.001722	8.99772	0.000000*	0.001933	8.015523	0.000000*	5.599158
	waU	0.038955	0.005347	7.285947	0.000000*	0.005486	7.101375	0.000000*	1.688294
	wbU	0.089159	0.00763	11.684586	0.000000*	0.007011	12.716807	0.000000*	2.590829
	gU	0.018026	0.002516	7.165732	0.000000*	0.002687	6.708585	0.000000*	1.441601
	aU_S	− 0.012246	0.001633	− 7.501131	0.000000*	0.001417	− 8.644688	0.000000*	1.117593
	dZ1L3_Z1L2	− 0.036889	0.001749	− 21.091218	0.000000*	0.001982	− 18.6096	0.000000*	5.385152
	waZ1L3_Z1L2	− 0.032016	0.00547	− 5.852958	0.000000*	0.004519	− 7.084758	0.000000*	1.155435
	wbZ1L3_Z1L2	− 0.090258	0.00753	− 11.985711	0.000000*	0.006917	− 13.048151	0.000000*	1.344078
Pb	Intercept	0.139901	0.056644	2.469836	0.013533*	0.051715	2.705229	0.006843*	——
	DU	− 0.014943	0.000736	− 20.301551	0.000000*	0.000729	− 20.5027	0.000000*	5.599158
	WAU	0.013655	0.002285	5.974566	0.000000*	0.002873	4.753298	0.000003*	1.688294
	WBU	0.006434	0.003262	1.972541	0.048587*	0.003156	2.038378	0.041546*	2.590829
	GU	0.00353	0.001075	3.28298	0.001050*	0.001167	3.024284	0.002515*	1.441601
	AU_S	− 0.00257	0.000698	− 3.682943	0.000246*	0.00068	− 3.78155	0.000169*	1.117593
	DZ1L3_Z1L2	0.009998	0.000748	13.37293	0.000000*	0.000699	14.29696	0.000000*	5.385152
	WAZ1L3_Z1L2	0.003429	0.002338	1.466585	0.142557	0.0016	2.142692	0.032164*	1.155435
	WBZ1L3_Z1L2	− 0.031554	0.003219	− 9.802628	0.000000*	0.002523	− 12.5072	0.000000*	1.344078

Table 3. OLS diagnosis

Zn	Number of observations	5944	Akaike's information criterion (AICc) [d]:	26815.8506
	Multiple *R*-squared [d]:	0.1500	Adjusted *R*-squared [d]:	0.1488
	Joint *F*-statistic [e]:	130.9000	Prob(> F), (8,10800) degrees of freedom:	0.000000*
	Joint Wald statistic [e]:	1667.8146	Prob(> Chi-squared), (8) degrees of freedom:	0.000000*
	Koenker (BP) statistic [f]:	579.0796	Prob(> Chi-squared), (8) degrees of freedom:	0.000000*
	Jarque–Bera statistic [g]:	514.8886	Prob(> Chi-squared), (2) degrees of freedom:	0.000000*
Pb	Number of observations	5944	Akaike's information criterion (AICc) [d]	16712.16432
	Multiple *R*-squared [d]	0.165207	Adjusted *R*-squared [d]	0.164082
	Joint *F*-statistic [e]	146.818393	Prob(> F), (8,5935) degrees of freedom	0.000000*
	Joint Wald statistic [e]	1286.157371	Prob(> Chi-squared), (8) degrees of freedom	0.000000*
	Koenker (BP) statistic [f]	454.780416	Prob(> Chi-squared), (8) degrees of freedom	0.000000*
	Jarque–Bera statistic [g]	9445.065151	Prob(> Chi-squared), (2) degrees of freedom	0.000000*

mineralization and its affecting factors very well. The Koenker (BP) statistic in Table 3 indicates that the model has statistically significant heteroscedasticity or inequalities.

All of these results show that the OLS model needs to be extended using the GWR model in order to describe better the non-stationary relationship between mineralization and its determinants.

Comparison between GWR and OLS Results

In this study, tricube and bisquare kernel functions of the GWR model are employed in 3D space, and both CV and AIC methods are adopted to determine the optimal nearest neighbors. The simulation calculation is implemented using MATLAB and the Econometrics Toolbox 7.0 (LeSage and Pace 2009) with modifications and extension to 3D made by us.

Comparison of Model Performance Between OLS and GWR

In this study, we measure the performance of models using *R*-squared (R^2) and adjusted R^2 values, which show how well the local regression model fits the dependent value (Lee and Schuett 2014). The R^2 and adjusted R^2 values of GWR and OLS are shown in Table 4. It is obvious that the GWR models perform better than the OLS model. All adjusted R^2 values in the GWR models for Zn grade are bigger than 0.70, far bigger than 0.15, the adjusted R^2 value in the OLS model for Zn grade. Similarly, all adjusted R^2 values in GWR models for Pb grade are also much bigger than that in OLS model. It can be concluded that the GWR models provide more specific and reliable information than the OLS model (Table 4). This shows that models considering local differences of factors can achieve higher reliability and, therefore, that spatial non-stationary between the mineralization and its affecting factors does exist. However, there may be some other factors not considered in our models.

Table 4 also shows the GWR results of two different kernel functions. The adjusted R^2 values of the GWR model for Zn grade with tricube and bisquare kernels are about 0.71 and 0.74, respectively, and those of the model for Pb grade are 0.68 and 0.77. It is obvious that the bisquare kernel function performs better than the tricube kernel function. These results demonstrate that the bisquare kernel function can reflect better the attenuation law of affecting factors with distance, and illustrate that the spatial non-stationary between the mineralization and its affecting factors is very prominent. Because the bisquare kernel performs better than the tricube kernel, the former is selected for GWR models in the subsequent analysis.

Comparison of Residuals Obtained by OLS and GWR

Residuals are the differences between the observed *y* values and the predicted *y* values. They provide a simple way to detect the spatial varying relationships between mineralization and its related factors for GWR or OLS model. Figure 3a and b depicts the residuals distribution of the OLS and GWR models for Zn grade, and Figure 3a and b

Table 4. Performance comparison of different models

	MODEL	Min_nNNs	Max_nNNs	Step	R^2	Adjusted R^2	Optimal nNNs
Zn	OLS				0.1500	0.1488	
	GWR (tricube)	30	1000	2	0.7076	0.7072	70
	GWR(bisquare)	30	1000	2	0.7450	0.7447	90
Pb	OLS				0.165	0.164	
	GWR (tricube)	30	1000	2	0.6838	0.6834	64
	GWR(bisquare)	30	1000	2	0.7693	0.7690	108

nNNs represents number of nearest neighbors

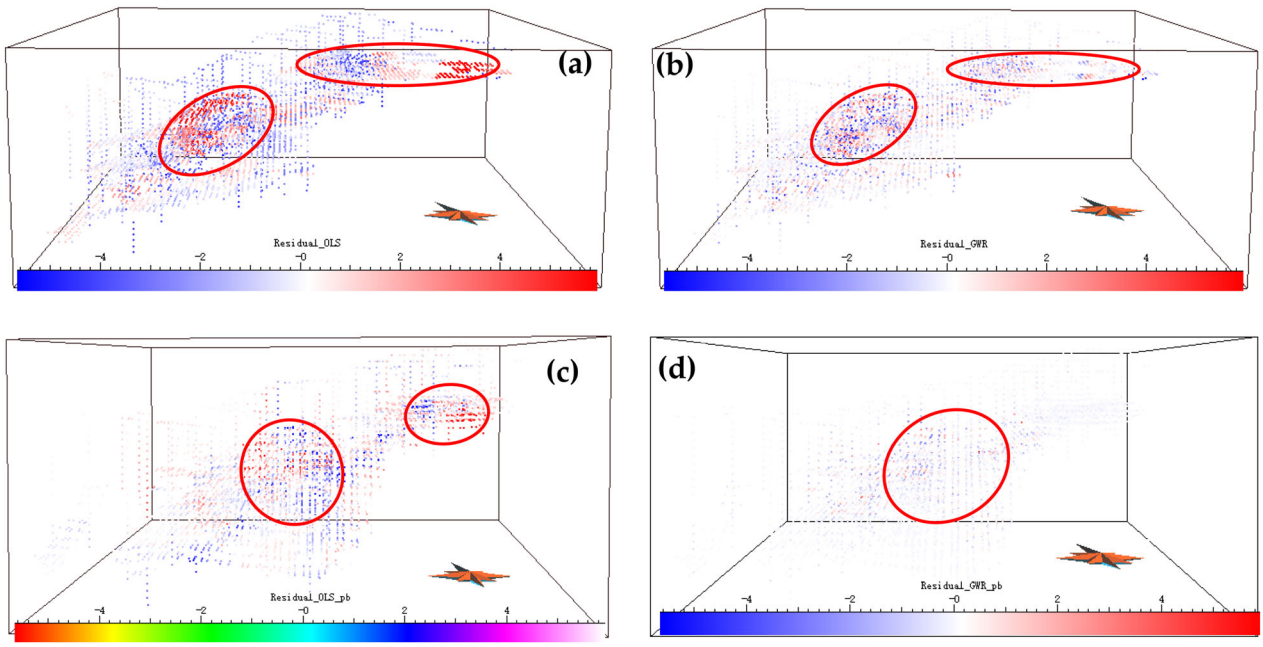

Figure 3. Residuals of (**a**) OLS and (**b**) GWR models for Zn, (**c**) OLS and (**d**) GWR models for Pb.

depicts the residuals distribution of OLS and GWR for Pb grade. The residuals derived of the GWR models are relatively small (Fig. 3b and d), indicating better performance in predicting the dependent variable, whereas the larger residuals of the OLS model (Fig. 3a and c) indicate lower performance in predicting the dependent variable.

Moreover, the spatial distribution of residuals of GWR models may provide some useful clues for the factors affecting mineralization in Dingjiashan Pb–Zn deposit. If the residual equals zero, it may indicate that the eight independent variables can fully describe the mineralization; otherwise, it can be inferred that the mineralization might be affected by other geological processes and more factors should be taken into consideration (Zhao et al. 2013).

The sizes of the residuals change with the spatial position. Larger residuals are present in two regions (the red elliptical regions in Fig. 3), which may be another indication of the existence of spatial non-stationarity between the mineralization and the factors that affect it.

Comparison of Spatial Autocorrelations of Residuals Obtained by OLS and GWR

If an OLS model has a spatial autocorrelation problem, GWR can help reduce it. On the other hand, if an OLS model does not have this problem, the application of GWR may increase spatial autocorrelation (Tu and Xia, 2008). The global Moran's I and local Moran's I of residuals for both the OLS

and GWR model are computed to measure the ability to deal with the spatial dependence.

Table 5 shows global Moran's I statistics on the residuals from OLS and GWR models. The global Moran's I of OLS is 0.0725 for Zn and 0.0650 for Pb, which indicates a slight positive spatial autocorrelation. Moran's I statistics of residuals from GWR is 0.0296 for Zn and 0.0286 for Pb, which shows a very weak spatial autocorrelation. The global Moran's I obtained in the GWR model is less than half of that in the OLS model, which illustrates that GWR models reduce the autocorrelation in comparison with OLS models.

Global autocorrelation is a general description of the whole space, but is only valid for homogeneous space. It becomes unreliable when the spatial process is heterogeneous. Local autocorrelation can solve this problem. Table 6 displays the statistical result for local Moran's I, in which the indices of OLS models indicate that the distribution is not uniform. Figure 4 shows local Moran's I distributions in the OLS and GWR models for Zn and Pb. The Moran's I distributions in the OLS model (Fig. 4a and c) show the spatial variability through space. Despite that the Moran's I is small in the global models, some regions with high values (e.g., the red elliptical regions in Fig. 4a and c) are consistent with the distribution of ore grade. The spatial distribution of Moran's I in the GWR model (Fig. 4b and d) is clearly more even than that in the OLS model.

All of the above-described results illustrate that the GWR models represent better the relationships by reducing the spatial autocorrelations in residuals.

Table 5. Global spatial autocorrelation of residuals

	Data object	Global Moran'I value	*Z*-score
Zn	Residuals of OLS	0.0725	15.7777
	Residuals of GWR	0.0296	6.4489
Pb	Residuals of OLS	0.0650	14.1425
	Residuals of GWR	0.0286	6.2386

Spatially Varying Relationships Between Mineralization and its Determinants

The local R^2 values and the values of t tests on the local parameter estimates for the GWR model can be calculated to explore the spatial variability between the mineralization and the controlling factors (Tu and Xia 2008). The local R^2 values for GWR change with the spatial position, ranging from − 0.2826 to 0.9992 (Fig. 5), which may be an indication of the existence of spatial variability between the mineralization and the factors that affect it. Higher R^2 values are mainly present in two regions (the red elliptical regions in Fig. 5), which are consistent with the mineral concentrations.

In statistics, the t-statistic is the ratio of the departure of the estimated value of a parameter from its hypothesized value to its standard error. Generally, a t-value that is greater than 1.96 or less than − 1.96 indicates a significant difference at the 95% confidence level. In this study, the t-statistic values for GWR exhibit an obvious spatial variability. The differences are mainly significant in two regions (the red elliptical regions in Fig. 6), and not significant in most of the other sites, suggesting that these controlling factors are less important for mineralization outside of the two concentrated areas.

Spatial Stationarity Test

Spatial Stationary Index Test

A spatial stationary index test of local parameter estimates was conducted to determine whether each explanatory variable shows significant geographical variability. The results of the test are presented in Table 7. The values are far bigger than 1, which confirms that the relationships between the mineralization and the eight explanatory variables are not uniform across space, and therefore, these variables should be modeled as local terms.

Table 6. Local spatial autocorrelation of residuals

	Model	Mean	Median	Mode	Variance	First quantile	Third quantile	Quartile deviation
Zn	OLS	1.47	0.2013	0.25	22.1362	− 0.0756	1.3631	1.4387
	GWR	0.01	0.0057	− 1.62	0.5839	− 0.0397	0.1177	0.1574
Pb	OLS	0.0000	− 0.1849	− 1.8605	0.9986	− 0.6389	0.4536	1.0925
	GWR	0.0163	0.0125	0.0000	0.2680	− 0.0920	0.1425	0.2345

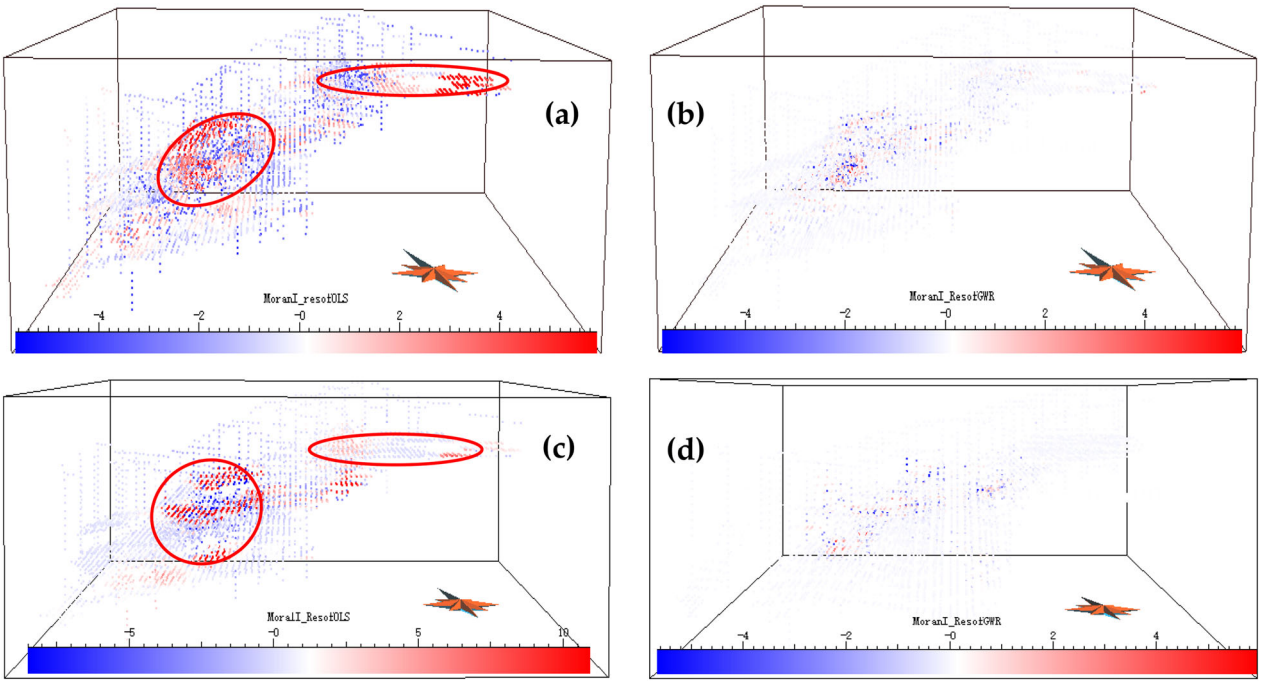

Figure 4. Comparison of local Moran's I: (**a**) OLS and (**b**) GWR models for Zn; (**c**) OLS and (**d**) GWR models for Pb.

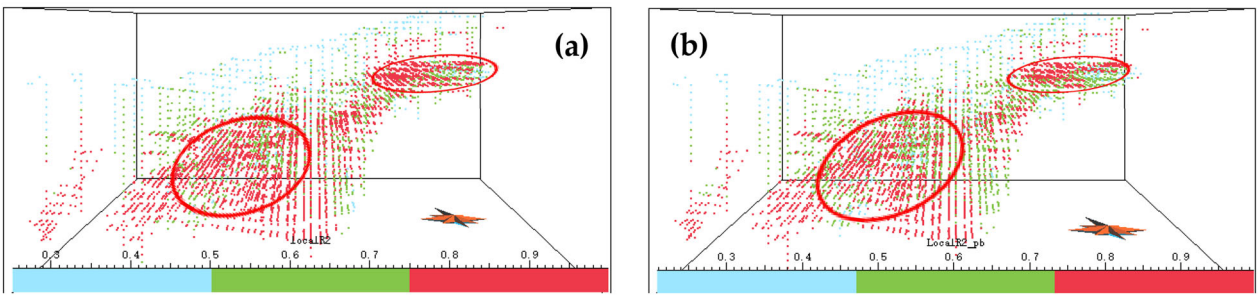

Figure 5. Local R^2 of GWR models for (**a**) Zn and (**b**) Pb.

Monte Carlo Non-stationarity Test

Monte Carlo significance test procedures consist of the comparison of the observed data with random samples generated by the hypothesis being tested (Hope 1968). As a Monte Carlo significance test is rather computationally intensive, we select a relatively inefficient Zn grade model with lower R^2 value to complete the test. In this paper, we consider the practical dataset as the observed value. The randomized dataset is generated by randomly changing the corresponding orders of the coordinates and variables. In Table 8, we report the results of a Monte Carlo test on the local parameter estimates for 1000 random samples. The p values of all the variables are less than 0.05, which indicates that there is significant spatial variation in the local parameter estimates for all the variables.

Figure 7 shows the comparison of GWR results between the practical dataset and the randomized dataset. The results shown in Figure 7a are for GWR simulations on the randomized dataset that are performed with different maximum bandwidths of 100, 300, 2000, and 5900, which can generate different results. Simulations 1, 2, 3, and 4 correspond to maximum bandwidths of 100, 300, 2000,

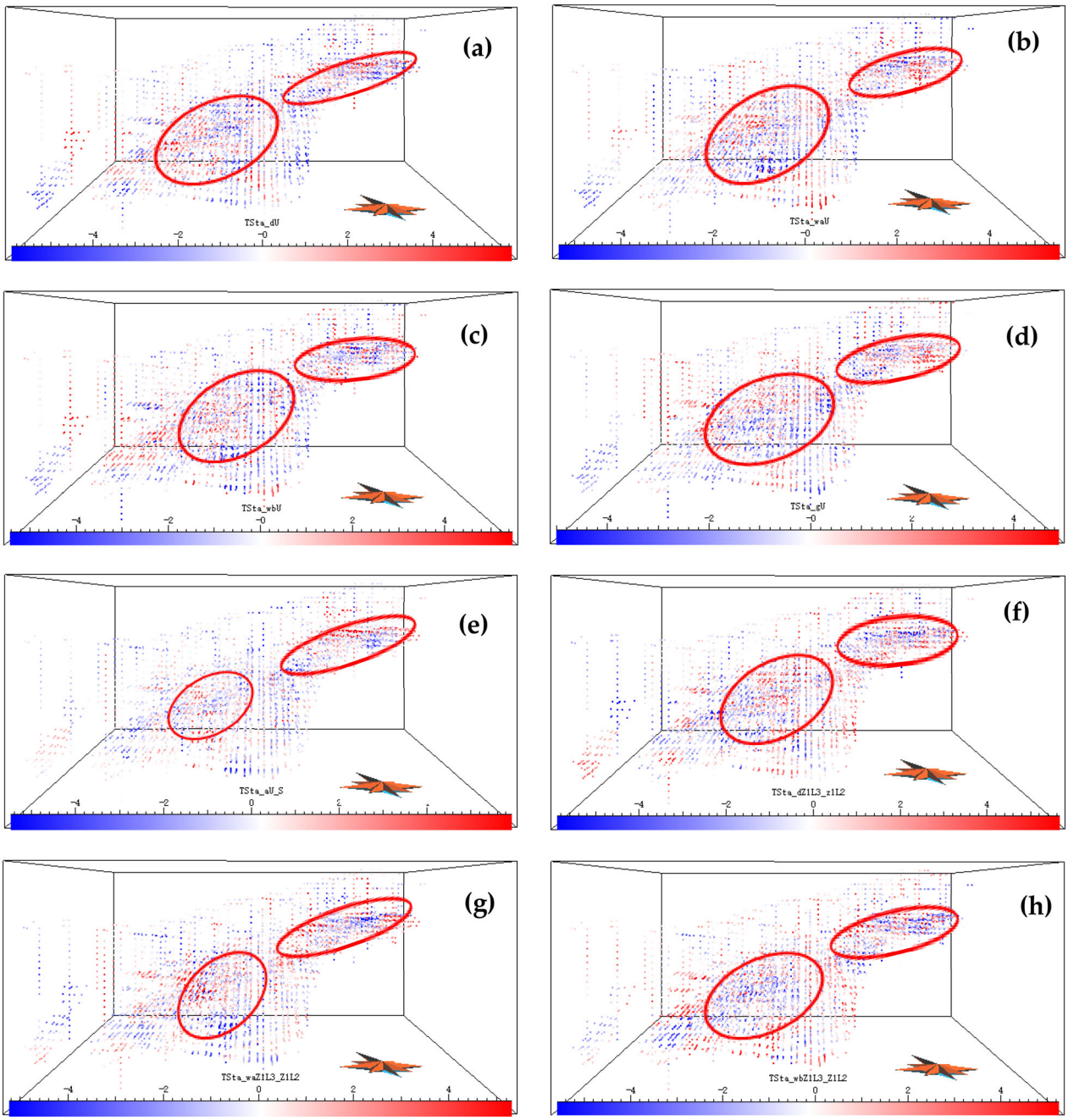

Figure 6. *T*-statistic of the parameter estimates (**a**) dU, (**b**) waU, (**c**) wbU, (**d**) gU, (**e**) aU_S, (**f**) dZ1L3_Z1L2, (**g**) waZ1L3_Z1L2, (**h**) wbZ1L3_Z1L2.

and 5900. From the radar chart in Figure 7a, we can see that the calculated optimal bandwidth increases synchronously with the increasing maximum bandwidth on the randomized dataset. The optimal bandwidth is almost equal to the given maximum bandwidth on the randomized dataset while it is fixed on the practical dataset. As the bandwidth tends to the maximum, the local model will tend to the global model. We interpret this to be because the relationships in the randomized dataset are uniform

Table 7. Stationary index of explanatory variables

	Variables	Intercept	dU	waU	wbU	gU	aU_S	dZ1L3_Z1L2	waZ1L3_Z1L2	wbZ1L3_Z1L2
Zn	Tricube	41.56	69.31	32.21	39.09	11.19	24.20	66.07	42.73	48.42
	Bisquare	42.80	61.82	28.60	34.82	10.53	20.15	59.20	39.20	41.29
	Mean	42.18	65.57	30.40	36.95	10.86	22.17	62.63	40.97	44.86
Pb	Tricube	29.04	39.36	27.17	31.16	8.72	13.94	39.31	43.26	38.43
	Bisquare	37.17	36.12	25.21	29.06	8.34	12.07	36.91	39.91	37.20
	Mean	33.10	37.74	26.19	30.11	8.53	13.00	38.11	41.59	37.82

Table 8. Monte Carlo test for spatial non-stationarity on Dingjiashan practical data

Variance	Intercept	dU	waU	wbU	gU	aU_S	dZ1L3_Z1L2	waZ1L3_Z1L2	wbZ1L3_Z1L2
p value	0.000	0.000	0.000	0.000	0.000	0.000	0.000	0.000	0.000

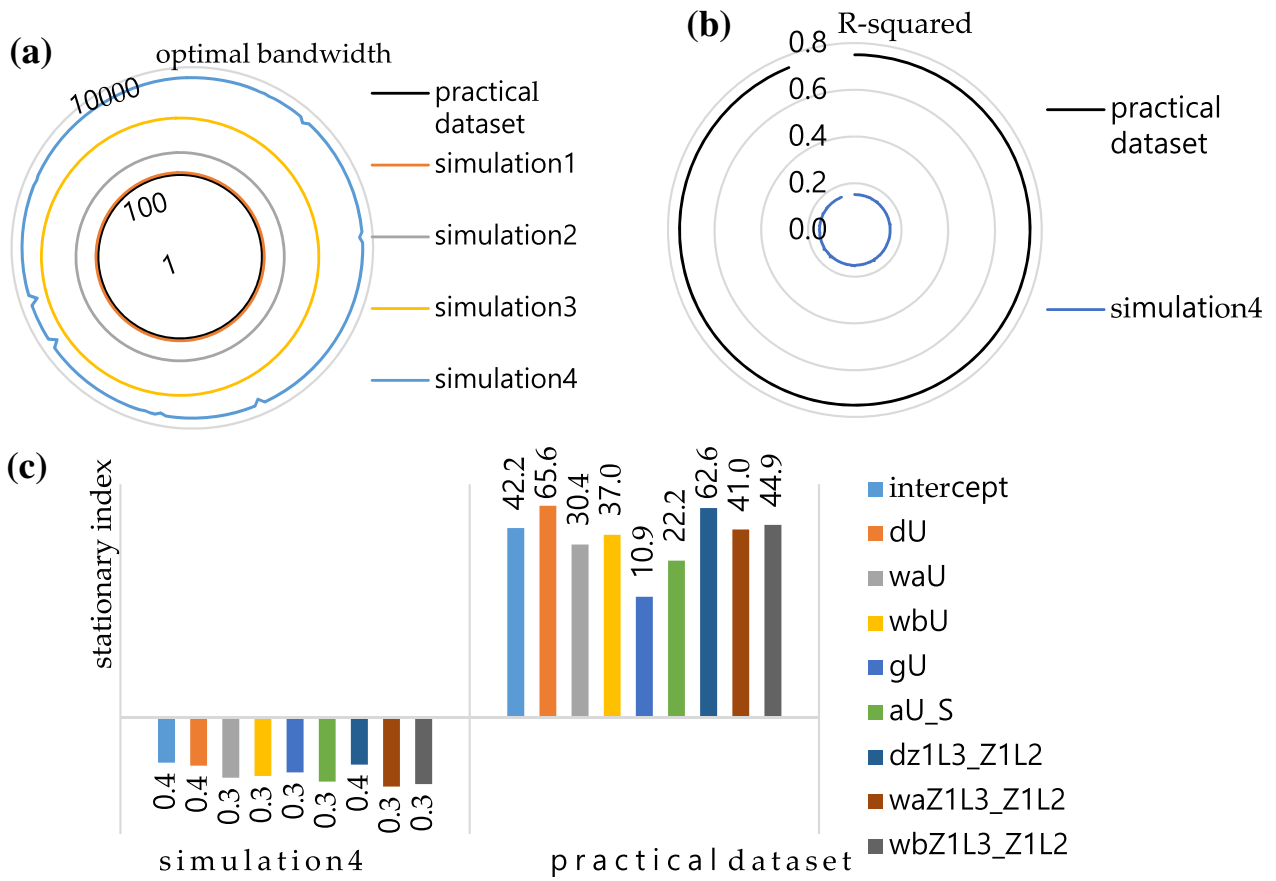

Figure 7. Monte Carlo simulation results of (**a**) optimal bandwidth, (**b**) *R*-squared, and (**c**) stationary index.

in space while they are non-stationary in the practical dataset.

As the maximum bandwidth should be set to *n* in order to obtain an optimal bandwidth in a GWR simulation, simulation 4 is adopted for comparison in the following analysis. Figure 7b shows the *R*-squared values for the randomized dataset and practical dataset. Obviously, the practical dataset

has a better performance, which demonstrates that non-stationary relationship is greater in the practical dataset than a randomized dataset. From Figure 7c, we can find that the stationary indexes of all the explanatory variables on the randomized dataset are less than 1, which proves their spatial stationarity. On the other hand, the indexes of all the explanatory variables are far greater than 1 on the practical dataset, which illustrates their non-stationarity in the practical dataset.

All these results reinforce the above conclusion of the existence of non-stationarity between the mineralization and its controlling factors in the Dingjiashan practical dataset.

DISCUSSION AND FUTURE WORK

Local parameter estimates of the GWR analysis indicate the relationships between the mineralization and its controlling factors. The results described above demonstrate the existence of non-stationary influence between the mineralization and the ore-controlling factors in the Dingjiashan practical dataset. Here we will further discuss the degree of non-stationary influence. Because of space limitations, we only take the Zn grade model for an example.

Table 9 shows the statistics for local parameter estimates in the GWR model. The parameter estimates of all the variables vary considerably from negative to positive values, which underline the non-stationary influence on mineralization by the ore-controlling factors. Figure 8 displays the spatial distribution of each explanatory variable and its parameter estimates. From these data and figures, we can find:

(1) Different from the explanatory variables, the corresponding parameter estimates of each variable vary through space from negative to positive. The larger values of most parameter estimates are concentrated in two areas (the red elliptical regions in Fig. 8) which are mostly consistent with the mineral concentrations. This reflects that the ore-controlling factors have more influence on the mineralization in these two areas.
(2) The parameter estimates of each variable vary in size. Generally, the larger values represent a closer relationship and a larger influence. In Table 9, both inner and outer interquartile ranges are employed to explore further the distribution trends of parameter estimates. The inner interquartile range is defined as the distance from the first to the third quartile, which is used to evaluate the less influential non-concentration areas. On the other hand, the outer interquartile range, which is the summed distance from the minimum to the first quartile and from the third quartile to the maximum, is used to evaluate the highly concentrated areas.

In the areas of high mineral concentration, the eight ore-controlling factors can be roughly divided into three classes by the outer interquartile range. The first class includes waZ1L3_Z1L2, wbZ1L3_Z1L2, which represent the trend–undulation of Z1L3_Z1L2 stratigraphic interface. The second class includes wbU, waU, and aU_S, which represent the trend–undulation of unconformity and

Table 9. Statistics of local parameter estimates for the GWR model

	dU	waU	wbU	gU	aU_S	dZ1L3_Z1L2	waZ1L3_Z1L2	wbZ1L3_Z1L2
Number	5944	5944	5944	5944	5944	5944	5944	5944
Mean	0.0047	− 0.0083	− 0.0786	− 0.0051	0.0301	− 0.0169	0.0950	− 0.0810
Variance	0.0830	0.3160	0.8410	0.0070	0.2020	0.0790	1.6660	1.2950
Minimum	− 1.4791	− 6.3309	− 8.3746	− 4.0909	− 7.9436	− 1.7152	− 10.3244	− 19.8220
Maximum	1.7978	4.7654	6.0717	0.3291	9.9847	1.6234	17.4016	7.1119
First quartile	− 0.1145	− 0.1350	− 0.2875	− 0.0278	− 0.0317	− 0.1091	− 0.1816	− 0.3939
Median	− 0.0090	0.0115	− 0.0019	− 0.0002	0.0027	− 0.0020	0.0107	− 0.0614
Third quartile	0.0984	0.1708	0.2439	0.0252	0.0341	0.0980	0.2473	0.2280
Interquartile range_inner	0.2129	0.3058	0.5314	0.053	0.0658	0.2071	0.4289	0.6219
Interquartile range_outer	3.4898	11.4021	14.9777	4.473	17.9941	3.5457	28.1549	27.5558

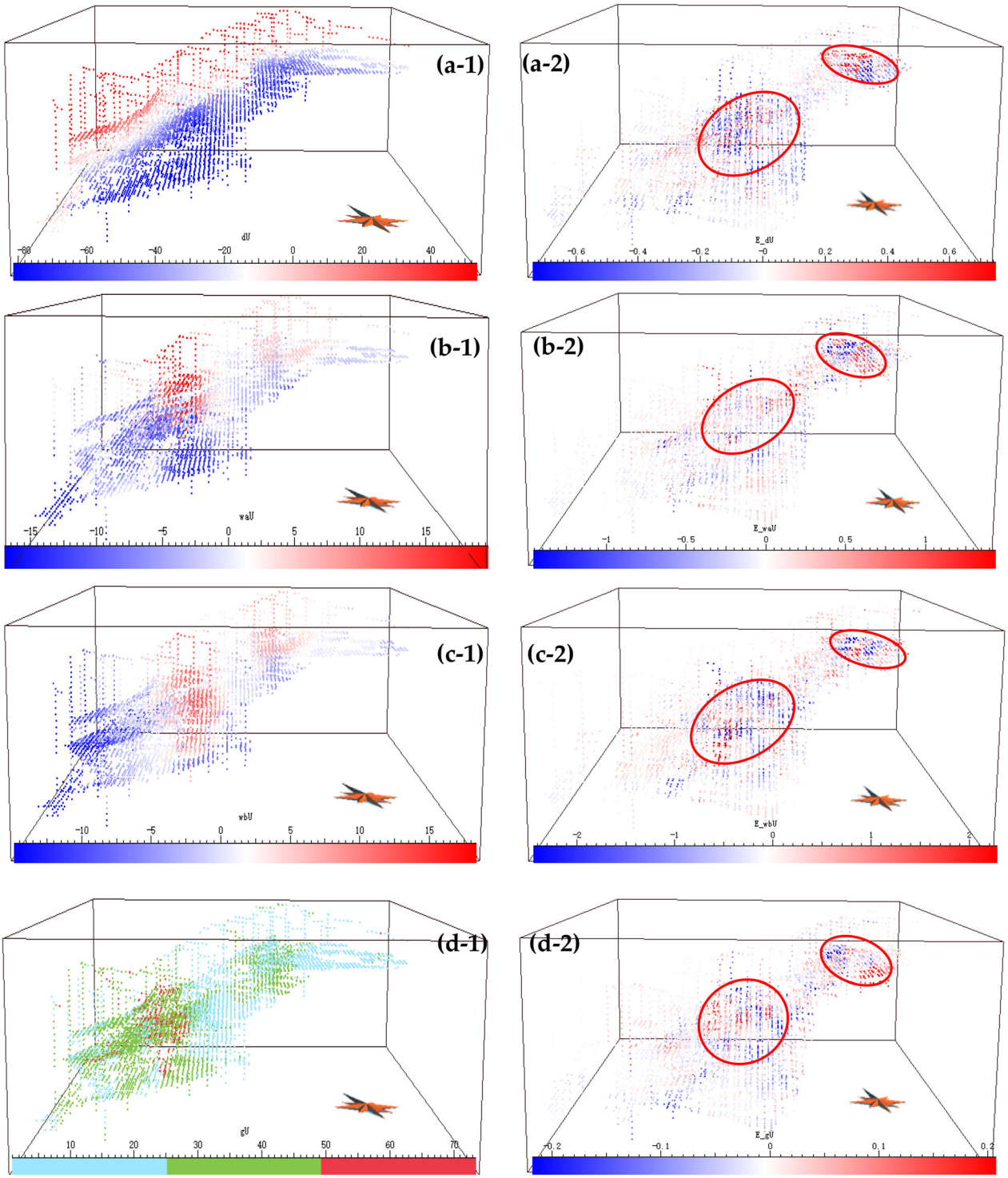

Figure 8. Spatial distribution of explanatory variables (**a-1**) dU, (**b-1**) waU, (**c-1**) wbU, (**d-1**) gU, (**e-1**) aU_S, (**f-1**) dZ1L3_Z1L2, (**g-1**) waZ1L3_Z1L2, (**h-1**) wbZ1L3_Z1L2 and the parameter estimates (**a-2**) dU, (**b-2**) waU, (**c-2**) wbU, (**d-2**) gU, (**e-2**) aU_S, (**f-2**) dZ1L3_Z1L2, (**g-2**) waZ1L3_Z1L2, (**h-2**) wbZ1L3_Z1L2.

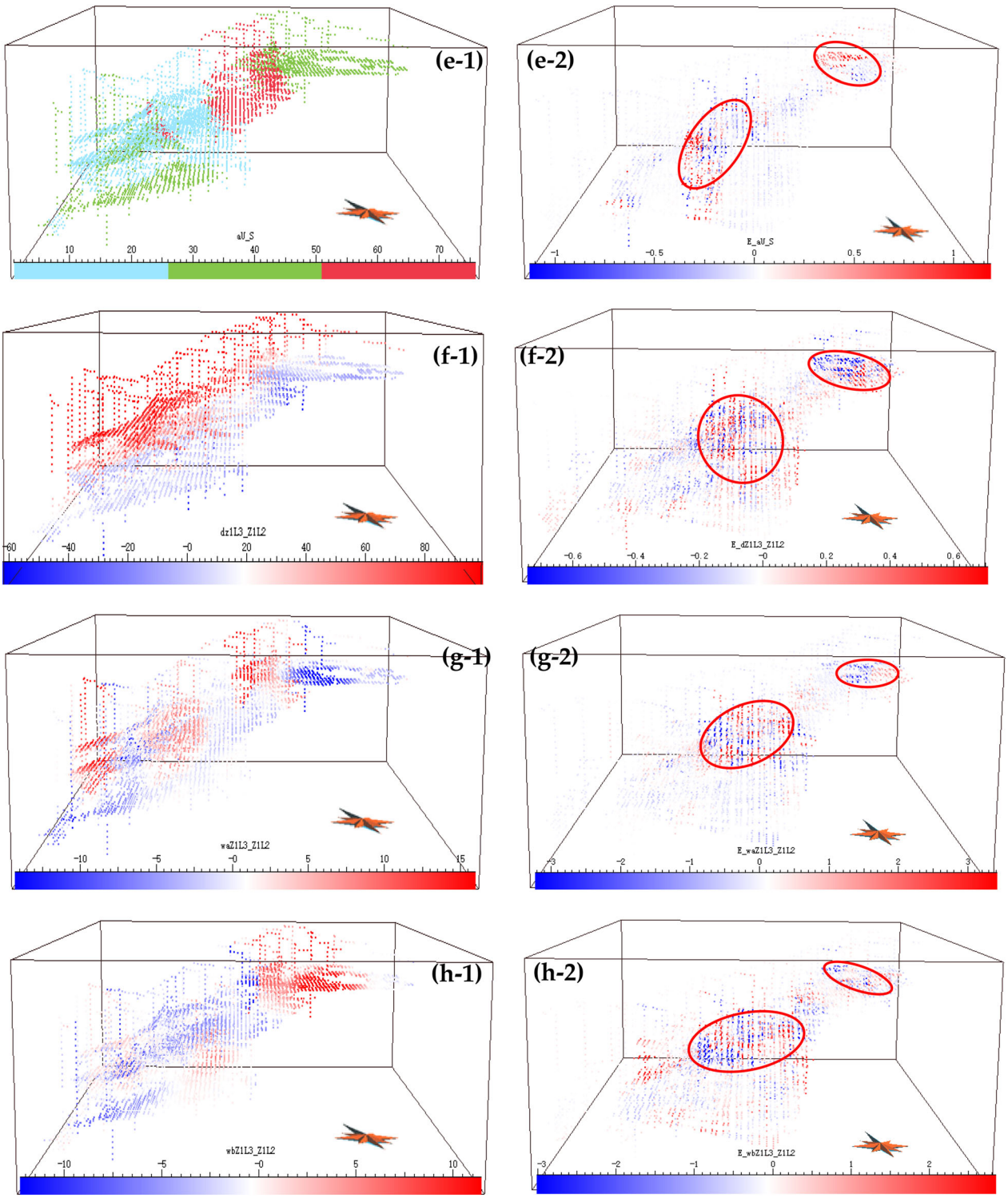

Figure 8. continued.

the angle of unconformity. The third class consists of dU, dz1L3_Z1L2, and gU, which are the distance to the Z1L3_Z1L2 stratigraphic interface, distance to the unconformity, and the slope of the unconformity. From these analyses, we can conclude that the trend–undulation of the stratigraphic interface has the greatest influence and trend–undulation of the unconformity and angle of the unconformity come second, while the distance to the stratigraphic interface, distance to the unconformity, and the slope of the unconformity are the weakest.

In the low mineral concentration areas, the ore-controlling factors are classified by the inner interquartile range. The first class includes waZ1L3_Z1L2, wbZ1L3_Z1L2, and wbU; the second class waU, dZ1L3_Z1L2, and dU; the third class includes gU and aU_S. These indicate to some degree that the trend–undulation of Z1L3_Z1L2 stratigraphic interface and the second-degree trend–undulation factor of the unconformity have the most influence on the mineralization while the slope and angle of the unconformity might not be as important in low mineral concentration areas. Through the whole space of Dingjiashan Zn deposit, we can find that waZ1L3_Z1L2 and wbZ1L3_Z1L2, the trend–undulation of Z1L3_Z1L2 stratigraphic interface, always attribute the most impact to the mineralization, but the slope of the unconformity has the weakest influence on the mineralization.

All the results and discussion presented here enhance our understanding of the formation of Zn deposits. Although the GWR model achieves better performance than other models, there still exist deficiencies. In the variable selection, there may exist other factors, which may contribute to the mineralization more appropriately. In the model application, the main defect may lie in the deep analysis and reasonable interpretation of the spatial variability of the regression coefficients in space from the GWR model. An appropriate solution would be to associate the regression coefficients with the metallogenic mechanism.

One suggestion for future research can be to enhance the interpolation and prediction abilities of GWR by introducing a kriging method for describing the structure of spatial variation in the GWR weight function. Another approach can focus on improving the predictions through integration with machine learning methods such as discriminant analysis, support vector regression, kernel regression, or neural networks.

CONCLUSIONS

Geographically weighted regression, which incorporates spatial location information into the regression model, is more conducive to exploring the interaction of spatial relations within geologically complex regions than ordinary linear regression. In this study, the results of statistical hypothesis tests and OLS fitting reveal that the ore-controlling factors selected in this study are highly statistically significant for the mineralization and that spatial non-stationarity between mineralization and its determinants does exist. Results of model comparisons prove that the GWR model has a better fit and higher prediction accuracy than the OLS model.

Quantitatively understanding the spatially varying relationships between geological factors and mineralization is crucial to metallogenic predictions. The regression coefficients obtained by GWR provide more information for geological interpretation. In this study, the parameter estimates indicate that the most influential controlling factor for the mineralization is the trend of the Z1L3_Z1L2 stratigraphic interface, and the weakest factor is the slope of the unconformity. The results reveal that the influence of the ore-controlling factors on mineralization varies considerably across the whole three-dimensional space, and it is stronger closer to the ore bodies and weaker further away.

In summary, this study described a new case study for the application of GWR in a three-dimensional area of geological significance. The conclusions from this study provide a reference for further research in predictive modeling.

ACKNOWLEDGMENTS

This research was funded by the National Key R&D Program of China (2017YFC0601503) and National Natural Science Foundation of China (41772349, 41472301, 41401532). The authors appreciate the amendments and suggestions for the paper from Professor A. Stewart Fotheringham of Arizona State University, and thank Dr. Ziqi Li and Dr. Hanchen Yu with whom discussions at Arizona State University greatly helped the research.

REFERENCES

Agterberg, F. P. (1964). Methods of trend surface analysis. *Colorado School Mines, 59,* 111–130.

Agterberg, F. P. (1970). Multivariate prediction equations in geology. *International Association for Mathematical Geology*, 319–324.

Andrew, B. T., Peter, J. K., & Sharmistha, B. S. (2015). Geographic variation in male suicide rates in the United States. *Applied Geography, 62,* 201–209.

Batisani, N., & Yarnal, B. (2009). Urban expansion in centre county Pennsylvania: spatial dynamics and landscape transformations. *Applied Geography, 29,* 235–249.

Breetzke, G. D., & Cohn, E. G. (2012). Seasonal assault and neighborhood deprivation in South Africa: some preliminary findings. *Environment and Behavior, 44*(5), 641–667.

Brunsdon, C., Fotheringham, A. S., & Charlton, M. E. (1996). Geographically weighted regression: a method for exploring spatial nonstationarity. *Geographical Analysis, 28,* 281–298.

Brunsdon, C., Fotheringham, A. S., & Charlton, M. (1998). Geographically weighted regression modeling spatial non-stationarity. *Statistician, 47,* 431–443.

Brunsdon, C., Fotheringham, A. S., & Charlton, M. (2002). Geographically weighted summary statistics - a framework for localized exploratory data analysis. *Computers, Environment and Urban Systems, 26,* 501–524.

Casetti, E. (1972). Generating models by the expansion method: Applications to geographic research. *Geographical Analysis, 4,* 81–91.

Chen, J. P., Wang, G. W., & Hou, C. B. (2005). Quantitative prediction and evaluation of mineral resources based on GIS: A case study in Sanjiang Region, Southwestern China. *Natural Resources Research, 14*(4), 285–294. https://doi.org/10.1007/s11053-006-9005-6.

Chen, Y., & Wu, W. (2017). Mapping mineral prospectivity using an extreme learning machine regression. *Ore Geology Reviews, 80,* 200–213.

Chen, Y., & Wu, W. (2019). Isolation forest as an alternative data-driven mineral prospectivity mapping method with a higher data-processing efficiency. *Natural Resources Research, 28*(1), 31–46. https://doi.org/10.1007/s11053-018-9375-6.

Cheng, Q. (1997). Fractal/multifractal modeling and spatial analysis. *Keynote Lecture in Proceedings of the International Mathematical Geology Association Conference, 1,* 57–72.

Cheng, Q. (1999). Multifractality and spatial statistics. *Computers & Geosciences, 25*(949–961), 1999.

Clement, F., Orange, D., Williams, M., Mulley, C., & Epprecht, M. (2009). Drivers of afforestation in Northern Vietnam: assessing local variations using geographically weighted regression. *Applied Geography, 29*(4), 561–576.

Fotheringham, A. S., & Brunsdon, C. (1999). Local forms of spatial analysis. *Geographical Analysis, 31,* 340–358.

Fotheringham, A. S., Brunsdon, C., & Charlton, M. (2002). *Geographically weighted regression: The analysis of spatially varying relationships* (1st ed.). Chichester: Wiley.

Fotheringham, A. S., Charlton, M., & Brunsdon, C. (1996). The geography of parameter space: an investigation of spatial non-stationarity. *International Journal of Geographical Information Science, 10,* 605–627.

Fotheringham, A. S., Charlton, M., & Brunsdon, C. (1998). Geographically weighted regression: A natural evolution of the expansion method for spatial data analysis. *Environment and Planning A, 30,* 1905–1927.

Fotheringham, A. S., Charlton, M. E., & Brunsdon, C. (2001). Spatial variations in school performance: A local analysis using geographically weighted regression. *Geographical and Environmental Modelling, 5,* 43–66.

Gao, J. B., & Li, S. C. (2011). Detecting spatially non-stationary and scale-dependent relationships between urban landscape fragmentation and related factors using Geographically Weighted Regression. *Applied Geography, 31,* 292–302.

Geri, F., Amici, V., & Rocchini, D. (2010). Human activity impact on the heterogeneity of a Mediterranean landscape. *Applied Geography, 30,* 370–379.

Gilbert, A., & Chakraborty, J. (2011). Using geographically weighted regression for environmental justice analysis: Cumulative cancer risks from air toxics in Florida. *Social Science Research, 40*(1), 273–286.

Harris, P., & Brunsdon, C. (2010). Exploring spatial variation and spatial relationships in a freshwater acidification critical load data set for Great Britain using geographically weighted summary statistics. *Computers & Geosciences, 36*(1), 54–70.

Hope, A. C. A. (1968). A simplified Monte Carlo significance test procedure. *Journal of the Royal Statistical Society. Series B: Methodological, 30*(3), 582–598.

Jessell, M. W., Ailleres, L., & De Kemp, E. A. (2010). Towards an integrated inversion of geoscientific data: What price of geology? *Tectonophysics, 490*(3–4), 294–306.

Lee, K. H., & Schuett, M. A. (2014). Exploring spatial variations in the relationships between residents' recreation demand and associated factors: A case study in Texas. *Applied Geography, 53,* 213–222.

LeSage, J., & Pace, R. K. (2009). *Introduction to spatial econometrics*. CRC Press, Taylor & Francis Group, New York.

Li, N., Song, X., Li, C., & Chen, H. (2019). 3D geological modeling for mineral system approach to GIS-based prospectivity analysis: Case study of an MVT Pb–Zn deposit. *Natural Resources Research, 28,* 995. https://doi.org/10.1007/s11053-018-9429-9.

Lin, N., Chen, Y., & Lu, L. (2019). Mineral potential mapping using a conjugate gradient logistic regression model. *Natural Resources Research*. https://doi.org/10.1007/s11053-019-09509-1.

Lindsay, M. D., Aillères, L., Jessell, M. W., de Kemp, E., & Betts, P. G. (2012). Locating and quantifying geological uncertainty in three-dimensional models: Analysis of the Gippsland Basin, southeastern Australia. *Tectonophysics, 546–547,* 10–27.

Liu, Y. C., Li, Z. X., Laukamp, C., West, G., & Gardoll, S. (2013). Quantified spatial relationships between gold mineralisation and key ore genesis controlling factors, and predictive mineralisation mapping, St Ives Goldfield, Western Australia. *Ore Geology Reviews, 54,* 157–166.

Lu, X., & Bo, T. (2014). On the determinants of UK house prices. *International Journal of Economics and Research, 512,* 57–64.

Lu, B. B., Charlton, M., & Fotheringham, A. S. (2011). Geographically weighted regression using a non-Euclidean distance metric with a study on London House Price Data. *Procedia Environmental Sciences, 7*(8), 92–97.

Mao, X. C., Dai, T. G., Wu, X. B., & Zou, Y. H. (2009). The stereoscopic quantitative prediction of concealed ore bodies in the deep and marginal parts of crisis mines: A case study of the Dachang tin polymetallic ore deposit in Guangxi. *Geology in China, 36*(2), 424–435.

Mao, X. C., Zhang, B., Deng, H., Zou, Y. H., & Chen, J. (2016). Three-dimensional morphological analysis method for geologic bodies and its parallel implementation. *Computers & Geosciences, 96,* 11–22.

Mao, X. C., Zou, Y. H., Chen, J., Lai, J. Q., Peng, S. L., Shao, Y. J., et al. (2010). Three-dimensional visual prediction of concealed ore bodies in the deep and marginal parts of crisis mines: A case study of the Fenghuangshan ore field in Tongling, Anhui, China. *Geological Bulletin of China, 29*(2–3), 401–413.

Nilsson, P. (2014). Natural amenities in urban space—A geographically weighted regression approach. *Landscape Urban Plan, 121,* 45–54.

Schamper, C., Auken, E., & Sørensen, K. I. (2014a). Coil response inversion for very early time modeling of helicopter-borne time-domain electromagnetic data and mapping of near-surface geological layers. *Geophysical Prospecting, 62,* 658–674.

Schamper, C., Jørgensen, F., Auken, E., & Effersø, F. (2014b). Assessment of near-surface mapping capabilities by airborne transient electromagnetic data—An extensive comparison to conventional borehole data. *Geophysics, 79,* B187–B199.

Shao, Y., Ma, C., Mao, X. C., et al. (2010). *3-D visual prediction of Dingjiashan lead-zinc deposit*. Beijing: Geological Publishing House.

Tobler, W. R. (1979). Smooth pycnophylactic interpolation for geographical regions. *Journal of the American Statistical Association, 74,* 519–530.

Tu, J., & Xia, Z. G. (2008). Examining spatially varying relationships between land use and water quality using geographically weighted regression I: Model design and evaluation. *Science of the Total Environment, 407*(1), 358–378.

Wang, W., Zhao, J., & Cheng, Q. (2015). GIS-based mineral exploration modeling by advanced geo-information analysis methods in southeastern Yunnan mineral district, China. *Ore Geology Reviews, 71,* 735–748.

Yao, J., & Fotheringham, A. S. (2015). Local spatiotemporal modeling of house prices: A mixed model approach. *Professional Geographer, 68*(2), 1–13.

Zhang, D., Cheng, Q., Agterberg, F. P., & Chen, Z. (2016). An improved solution of local window parameters setting for local singularity analysis based on excel vba batch processing technology. *Computers & Geosciences, 88*(C), 54–66.

Zhang, D., Jia, Q., Xu, X., Yao, S., Chen, H., Hou, X., et al. (2019). Assessing the coordination of ecological and agricultural goals during ecological restoration efforts: A case study of Wuqi County, Northwest China. *Land Use Policy, 82,* 550–562.

Zhang, B. Y., Mao, X. C., Zhou, S. G., Hu, C., & Yan, F. (2012). Spatial affecting extents limited comprehensive geo-information mineral resources quantitative prediction models: A case study of manages ore prediction in western Guangxi and southeastern Yunnan. *China. Geological review, 58*(5), 978–989.

Zhang, D., Ren, N., & Hou, X. (2018). An improved logistic regression model based on a spatially weighted technique (ILRBSWT v1. 0) and its application to mineral prospectivity mapping. *Geoscientific Model Development*, 11(6), 2525–2539.

Zhang, S. G., Shi, D. F., Han, S. L., & Li, G. X. (2011). Genetic mineralogical study of pyrrhotite in the Dingjiashan Pb-Zn ore district, Fujian province. *Journal of Mineralogical and Petrological Sciences, 31*(3), 11–17.

Zhao, J., Wang, W., & Cheng, Q. M. (2013). Investigation of spatially non-stationary influences of tectono-magmatic processes on Fe mineralization in eastern Tianshan, China with geographically weighted regression. *Journal of Geochemical Exploration, 134,* 38–50.

Zhao, J., Wang, W., & Cheng, Q. M. (2014). Application of geographically weighted regression to identify spatially non-stationary relationships between Fe mineralization and its controlling factors in eastern Tianshan, China. *Ore Geology Reviews, 57,* 628–638.

Zuo, R., Carranza, E. J. M., & Wang, J. (2016). Spatial analysis and visualization of exploration geochemical data. *Earth-Science Reviews, 158,* 9–18.

Zuo, R., & Xiong, Y. (2018). Big data analytics of identifying geochemical anomalies supported by machine learning methods. *Natural Resources Research, 27,* 5–13.